The CTNNBIP1-CLSTN1 fusion transcript regulates human neocortical development

Cell Reports

The CTNNBIP1-CLSTN1 fusion transcript regulates human neocortical development

Graphical abstract
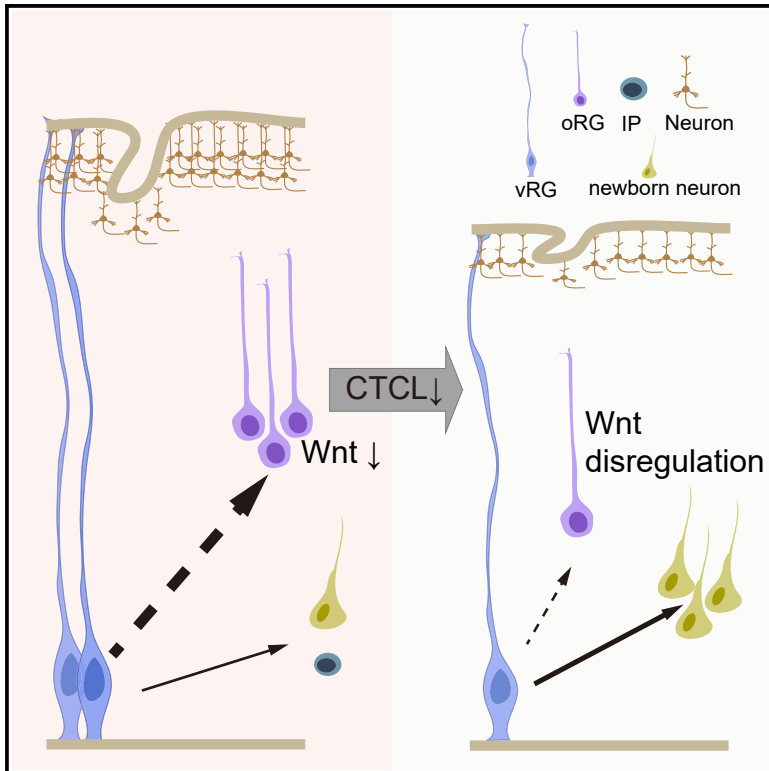
Authors

Min-Yi Ou, Qi Xiao, Xiang-Chun Ju,
Peng-Ming Zeng, Jing Huang,
Ai-Li Sheng, Zhen-Ge Luo

Correspondence

xiangchun.ju@oist.jp (X.-C.J.),
luozhg@shanghaitech.edu.cn (Z.-G.L.)

In brief

Ou et al. report the presence of fusion transcripts in distinct cell types of developing human cortex. They investigate the function of a human-specific fusion CTCL in cultured human cerebral organoids. Downregulation of CTCL impairs neural progenitor proliferation and organoid growth likely via dysregulation of the canonical Wnt/β-catenin signaling.

Highlights

- Fusion transcripts occur in developing human cortex in cell-type-specific manner.

- The CTCL fusion transcript is expressed in human cortical neural progenitors.

- CTCL tightly controls neural progenitor proliferation and neuronal differentiation.

- CTCL fine-tunes Wnt/β-catenin signaling in human cortical neural progenitors.

CellPress

Article

The CTNNBIP1-CLSTN1 fusion transcript regulates human neocortical development

Min-Yi Ou,[1,2,3,5,7] Qi Xiao,[2,3,7] Xiang-Chun Ju,[2,4,7,*] Peng-Ming Zeng,[1] Jing Huang,[1] Ai-Li Sheng,[2,6] and Zhen-Ge Luo[1,8,*]

[1]School of Life Science and Technology, ShanghaiTech University, Shanghai 201210, China
[2]Institute of Neuroscience, Center for Excellence in Brain Science and Intelligence Technology, Shanghai Institute for Biological Sciences, Chinese Academy of Sciences, Shanghai 200031, China
[3]University of Chinese Academy of Sciences, Beijing 100049, China
[4]Present address: Okinawa Institute of Science and Technology, Onna-son, Okinawa 904-0495, Japan
[5]Present address: Department of Plastic & Reconstructive Surgery, Shanghai Ninth People's Hospital, School of Medicine, Shanghai Jiao Tong University, Shanghai 200011, China
[6]Present address: Shanghai Institute of Nutrition and Health, Shanghai Institute for Biological Sciences, Chinese Academy of Sciences, Shanghai 200031, China
[7]These authors contributed equally
[8]Lead Contact
*Correspondence: xiangchun.ju@oist.jp (X.-C.J.), luozhg@shanghaitech.edu.cn (Z.-G.L.)
https://doi.org/10.1016/j.celrep.2021.109290

SUMMARY

Fusion transcripts or RNAs have been found in both disordered and healthy human tissues and cells; however, their physiological functions in the brain development remain unknown. In the analysis of deposited RNA-sequence libraries covering early to middle embryonic stages, we identify 1,055 fusion transcripts present in the developing neocortex. Interestingly, 98 fusion transcripts exhibit distinct expression patterns in various neural progenitors (NPs) or neurons. We focus on *CTNNBIP1-CLSTN1* (*CTCL*), which is enriched in outer radial glial cells that contribute to cortex expansion during human evolution. Intriguingly, downregulation of *CTCL* in cultured human cerebral organoids causes marked reduction in NPs and precocious neuronal differentiation, leading to impairment of organoid growth. Furthermore, the expression of *CTCL* fine-tunes Wnt/β-catenin signaling that controls cortex patterning. Together, this work provides evidence indicating important roles of fusion transcript in human brain development and evolution.

INTRODUCTION

The expansion of the cerebral cortex is thought to improve cognitive ability during the evolution of mammals, and this process involves an expanded neural progenitor pool and extended neurogenic period (Geschwind and Rakic, 2013; Sun and Hevner, 2014). Studies in mice have shown that radial glial cells (RGs) in the ventricular zone (VZ) and intermediate progenitors (IPs) in the subventricular zone are major types of neural progenitors (NPs) that give rise to cortical neurons in various developmental stages (Malatesta et al., 2000; Miyata et al., 2004; Noctor et al., 2001). Recent cross-species studies have shown the presence of heterogeneous types of NPs with high proliferation potency in the expanded subventricular zone (SVZ) in the developing primate cortex, and RGs localized in the outer SVZ constitute major types of basal NPs (Betizeau et al., 2013; Fietz et al., 2010; Hansen et al., 2010). Intriguingly, forced generation of these basal NPs, induced by modulating cell cycle progression (Nonaka-Kinoshita et al., 2013; Stahl et al., 2013) or overexpressing human linage-specific genes, promoted cortex expansion in mice (Florio et al., 2015; Ju et al., 2016; Liu et al., 2017) or non-human primate (Heide et al., 2020). Increased proliferative ability of cortical NPs,

including the ventricular RGs (vRGs), IPs, and basal or outer RGs (bRGs or oRGs) and prolonged duration of neurogenesis are believed to contribute to human cortical expansion (Lui et al., 2011; Sun and Hevner, 2014). Nevertheless, it remains obscure how the temporal progression of cortical neurogenesis is tightly controlled.

The human proteome is featured in several levels from gene transcription to translation. Of note, gene fusion caused by chromosomal translocation resulting in generation of novel fused proteins, has been considered as a major driving force for human cancers (Rabbitts, 1994). Fusion transcripts or chimeric RNA molecules, identified through reverse-transcription PCR (RT-PCR) or RNA sequencing (RNA-seq) methods, have been found in normal margins of neoplasia (Chase et al., 2010; Ren et al., 2014; Stransky et al., 2014; Yoshihara et al., 2015) and normal tissues in different species (Babiceanu et al., 2016; Huang et al., 2008; Lei et al., 2016a; Li et al., 2008; Tang et al., 2017). It is suggested that fusion transcripts might be derived from intergenic splicing rather than chromosomal rearrangement (Brooks et al., 2009; Finta and Zaphiropoulos, 2002; Horiuchi and Aigaki, 2006; Jia et al., 2016). Emerging lines of evidence suggest that some fusion transcripts, either protein-coding or

noncoding RNAs, function in physiological processes, such as regulating stem/progenitor cell differentiation or maintaining pluripotency of human embryonic stem cells (hESCs) (Brooks et al., 2009; Wu et al., 2014). In contrast to the conventional view that fusion transcripts are rare in non-cancer samples, indeed tens of thousands of fusion transcripts are present in various normal human tissues and cells with hundreds of them found recurrently (Babiceanu et al., 2016; Singh et al., 2020). Interestingly, only a small fraction of recurrent fusions is shared by mouse and human (Babiceanu et al., 2016), suggesting that chimeric fusion RNAs might provide another layer for distinctive transcriptional signature during evolution. The recent landscape studies of chimeric RNAs in various human tissues and cells have shown the occurrence of fusion transcripts in adult and aging human cortex (Mehani et al., 2020; Singh et al., 2020), but the functional relevance remains unclear.

In this work, we have demonstrated the presence of fusion transcripts in various neural cell types in the developing human cortex and performed functional analysis on a human-specific fusion *CTNNBIP1-CLSTN1* (*CTCL*), which has been shown to be generated by *cis*-splicing fusion of the first 5 exons of *CTNNBIP1* (β-Catenin-interacting protein1) and the last 17 exons of *CLSTN1* (Calsyntenin 1) (Babiceanu et al., 2016; Chwalenia et al., 2019). Given the recurrent detection of *CTCL* in normal human tissues and cells but not in mice (Babiceanu et al., 2016) and the enrichment of *CTCL* in oRGs, we analyzed the role of *CTCL* in human cortex development using cultured human cerebral organoids as the model system. We found that downregulation of *CTCL* significantly reduced proliferative NPs and caused precocious neuronal differentiation. Furthermore, *CTCL* fine-tunes Wnt signaling, which has been shown to be involved in cortex development. These results provide insight into the physiological function of chimeric RNA fusions in human brain development.

RESULTS

Fusion transcripts are widely expressed in the developing human cortex

To explore the fusion transcriptome in the developing human neocortex, we analyzed eight paired-end RNA-seq libraries covering five developmental stages, including gestational week (GW) 13, 14.5, 16, 21, and 23, of human cortices (GSE71315) (Liu et al., 2016) (Figure S1A), using SOAPfuse software (Jia et al., 2013). If junction reads and spanning reads were recognized simultaneously at least once (Figure S1B), the splicing events would be considered as positive fusion candidates. In total, 1,055 fusion transcripts were identified (Figures 1A, 1B, and S1C; Table S1). Considering that these RNA libraries were prepared with two different RNA extraction approaches, poly(A)-enriched mRNAs or total RNAs, we performed a comparison of fusion transcriptomes from poly(A)-enriched mRNAs and total RNAs to see whether mRNA enrichment influenced identification of fusions (Figures 1A–1F and S2A). As shown in Figure 1B, 602 and 638 fusion transcripts were identified from poly(A)-enriched mRNAs and total RNAs, respectively, and 185 fusions were shared by two groups, of which, 31%–58% fusions were detected at single time point (see also Figure S2B). Compared to total RNAs, the poly(A)-enriched mRNAs showed higher numbers of

splicing events per million mapped reads (SPMR) (Figure 1C) and more fusion transcripts per million mapped reads (FTPM) (Figure 1D), indicating that more fusion transcripts can be identified from mRNA-enriched extractions. Furthermore, poly(A)-enriched mRNAs contained more intrachromosomally fused transcripts, while total RNA extraction generated more interchromosomal fusion transcripts (Figures 1E and S1C). Fusion events were categorized according to the reading frames, and among all fusion types, only ~16.6% and ~10.5% were in-frame fusions in poly(A)-enriched mRNAs and total RNAs, respectively (Figure 1F). More events were frameshift fusions (~28.5% in poly(A)-enriched group and ~20.8% in total RNA group) and fusions between unknown isoforms of parental mRNAs (both) or bioinformatically undetermined (NA) (Figure 1F). Of the 1,055 fusion transcripts, 86% in-frame and 67% other fusions of parental genes produced only one fusion transcript (Figure 1G), and of the 185 fusions identified from both extracts, 96% in-frame and 78% other fusions of parental genes produced only one fusion transcript (Figure S2C).

Next, we examined the motifs covering 10-bp sequences immediately upstream or downstream to the fusion site of parental genes and found that the canonical GT/AG donor-acceptor motif had the highest position weight, regardless of the fusion outcome of downstream genes (Figure S2D). In line with this, protein-coding genes exhibited highest portion among all predicated fusion genes, although the category distribution had heterogeneity across different samples (Figures 1H and 1I) and the majority (~70%) of fusion transcripts were formed between two protein-coding genes. Since a database annotating the fusion transcript ontology is still lacking, we performed a normal GO enrichment analysis of all parental genes to explore potential roles of fusion transcripts in human cortex. We found that the biologic processes positively regulating neurogenesis and dendrite development were highly enriched (Figure S2E). This result suggests the potential function of fusion transcripts in neuronal development or network activity. For parental genes of 108 in-frame fusion transcripts identified by two RNA extractions, the GO enrichment analysis indicated their relationships with GTPase activity and GTP binding (Figure S2F). We next examined the relationship between the expression of fusion transcripts and their parental genes. We checked all 1,055 fusion transcripts and could not find a correlation between the expression level of fusion transcripts and parental genes, either upstream or downstream (Figures S2G and S2H). Thus, the expression of fusion transcripts is independent of parental genes. Many in-frame fusions were detected recurrently at specific cortical developmental stages with various expression levels (Figure 1J). This dynamic expression pattern suggests fine-tuning of complicated signaling network governing the developmental process of human cortex. To further check the presence of the full-length fusion transcripts in the developing human cortex, we performed long read sequencing and identified four fusion transcripts from GW17.0 human brain cortex, two of which were resulted from fusion of adjacent genes (Table S2). We also used ribosome profiling followed with RNA-seq (Ribo-seq) to evaluate the translation potential of fusion transcripts in the GW17.0 human brain cortex (Figure S2I; Table S2). We identified nine fusion transcripts from 9.8 million uniquely aligned reads with an average
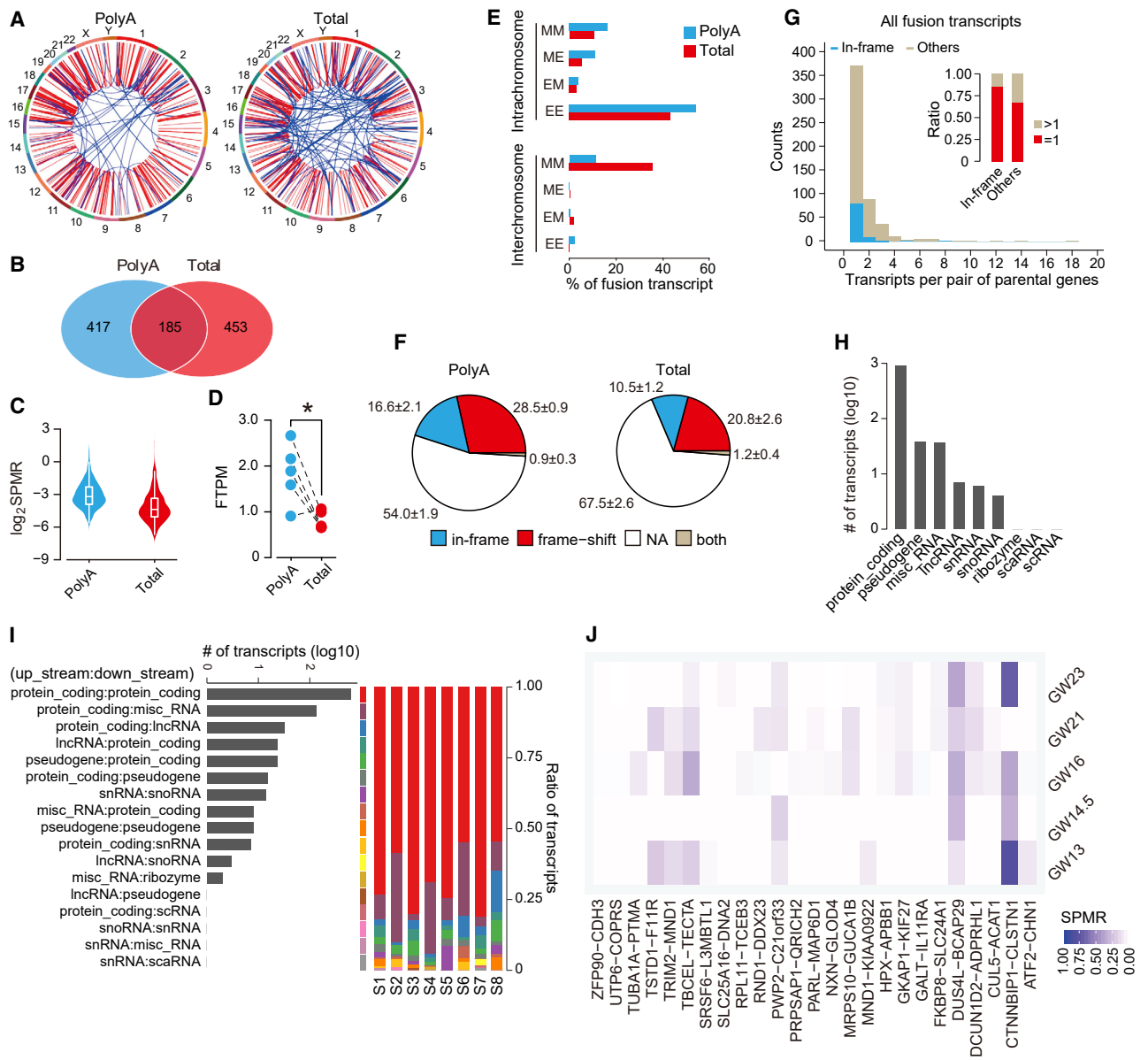
Figure 1. Expression of fusion transcripts in the developing human neocortex

(A) Circos plots of genomic distribution of fusion transcript parental genes observed in poly(A) and total RNA. Red lines indicate parental genes located in the same chromosome; blue lines indicate parental genes located in different chromosomes.

(B) Venn diagram illustrating shared and distinct fusion transcripts between poly(A) and total groups.

(C) Violin plots for SPMR values of fusion transcripts in poly(A) and total RNA.

(D) Quantification of fusion transcripts per million mapped reads (FTPM) in poly(A) and total RNA. *p < 0.05 (n = 5 cortices each group; paired t test).

(E) Types of fusions based on parental gene locations. MM: both sides fall into the middle of known exons; ME or EM: one side using known exon boundary and another side in the middle of known exon; EE: both sides using known exon boundaries. Intrachromosome: parental genes locate in the same chromosome; interchromosome: parental genes locate in different chromosomes.

(F) Distribution of the fusion transcripts according to their protein-coding potential: in-frame fusion, fused downstream gene can be encoded correctly; frameshift, downstream gene cannot be properly encoded with the introduction of an early stop codon; both, in-frame fusion or frameshift based on parental isoforms used; NA, undetermined by present algorithm. Data were presented as mean ± SEM.

(G) Quantification of fusion transcripts per pair of parental genes. Others, fusion transcripts annotated as frameshift, both, or NA.

(H) Biotype quantification of fusion transcripts. Misc_RNA, miscellaneous RNA; Tnc_RNA, tiny noncoding RNA; snRNA, small nuclear RNA; snoRNA, small nucleolar RNA; scaRNA, small Cajal body-specific RNA; scRNA, small cytoplasmic RNA.

(I) Biotype quantification of parental gene combinations in all samples (left panel) and individual samples (S1–8, right panel).

(J) Fusion transcripts expressed in denoted developing stages. GW, gestational weeks.

See also Figures S1–S3 and Tables S1 and S2.

Figure 2. Fusion transcripts in distinct cell populations of embryonic human prefrontal cortex

(A) Diagram of the four cell populations isolated in the embryonic human cortex. N, neurons; oRG, outer radial glia; IP, intermediate progenitor; vRG, ventricular radial glia.

(B) Expressional heatmap of cell markers measured by RNA-seq in individual cell populations.

(C) Circos plots of genomic locations of fusion parental genes in the four cell populations.

(D) Number of fusion transcripts per million mapped reads (FTPM) in each cell population.

(E) Violin and boxplots for expression levels of fusion transcripts across cell populations.

(F) Composition of fusion transcripts detected in four cell populations.

(G) Pearson analysis for the correlation of fusion transcripts and their parental genes. TPM, transcripts per kilobase million.

(H) Venn diagram for the overlaps of fusion transcript among different cell populations.

(I) Expressional heatmap of in-frame fusion and noncoding fusion transcripts in indicated cell populations.

See also Figure S3 and Tables S3 and S4.

sequence length of 27 bp. Four of nine (44%) were found to be in-frame fusions and others were frameshift or unknown mutations (Figure S2J; Table S2), which is consistent with the finding that highest ratio of in-frame fusions was formed between protein-coding parental genes. Whether these frameshift and unknown fusions encode functional products needs further investigation.

Cell-type-specific expression of fusion transcripts

To gain more insights into the expression patterns of fusion transcripts in different neural cell types involved in human cortex development, we sorted out three populations of NPs, including vRGs, oRGs, and IPs, as well as one population of neurons from GW14.5 prefrontal cortex by cytometry according to their valid markers (Figure 2A) (Pollen et al., 2015). The identities of sorted cell populations were further validated by their marker expressions (Figure 2B). Genetic abnormality of the sequenced sample was excluded by the SNPs/copy number variation (CNV) analysis of the RNA-seq data (McConnell et al., 2013) (Figures S3A–S3C and STAR Methods). We identified 43 candidates of fusion transcripts in oRGs, 6 in vRGs, 46 in IPs, and 25 in

Figure 3. Verification of *CTNNBIP1-CLSTN*1 expression

(A) Sanger sequencing of the fusion site in *CTNNBIP1-CLSTN1* (*CTCL*).

(B) Schematic diagram for the sites of primers used to identify CTCL and its parental transcripts. Arrows indicate primer sites in parental gene transcripts.

(C) The expressions of *CTCL* in indicated cell populations were quantified by qPCR. Data were presented as mean ± SEM of three biological repeats.

(D) RT-PCR analysis for the expression of *CTCL* in fetal cortex of human (GW14.5) and mouse (E14.5). h., human; m., mouse.

(E) Expression of CTCL protein in embryonic human cortex determined by immunoblotting with antibodies recognizing the N terminus of CTNNBIP1 or the C terminus of CLSTN1. Red arrowheads indicate the band of CTCL protein. Black arrow indicates the band of CLSTN1 protein.

(F) RT-PCR analysis for the expression of CTCL in human brain organoids cultured for different days. Scale bars, 500 μm.

SATB2$^+$ neurons (Figure 2C; Table S3). After normalization to mapped reads, we found that more fusion transcripts were identified in oRGs or IPs, compared to vRGs (Figure 2D). To determine whether the low occurrence of fusions in vRGs was due to low expression levels, we compared the SPMR values of fusion transcripts in four cell populations and found that vRG fusion transcripts exhibited the highest SPMR values compared to other populations (Figure 2E). Thus, the expression level had no effect on detection efficiency. Among these fusion events, around 8.2% were in-frame fusions (Figure 2F), indicating the potential for the expression of novel fusion proteins during human cortex development. Again, the expression level of fusion transcripts was not related with their parental genes (Figure 2G). Notably, only around 17.3% (17/98) fusions were expressed in more than one cell population, whereas majority of fusions were specifically expressed in only one population (Figure 2H). Among them, three in-frame fusions, *CTNNBIP1-CLSTN1*, *BICD2-IPPK*, and *NFATC2IP-SPNS1*, were enriched in oRGs, and *FAM111B-FAM111A* fusion was expressed in both oRGs and IPs cells (Figure 2I). Three in-frame fusion transcripts (two *MND1-KIAA0922* fusions with different fusion sites and one *UBA2-WTIP* fusion) were expressed merely in IPs, and three *LINC01158-LINC01114* noncoding fusions with different fusion sites were identified in SATB2$^+$ neurons (Figure 2I). Distinct types of fusions identified in different neural cell populations suggest specific roles of fusion transcripts or with some being heterogeneous "noisy" transcription process at various stages of neurogenesis, which needs to be explored further. We also analyzed fusion transcripts in single oRG cell by surveying two published single-cell RNA sequencing (scRNA-seq) datasets (Liu et al., 2017; Zhong et al., 2018). We identified a few fusion transcripts in a small fraction of oRGs (7/45), with fusion numbers ranging from 0 to 5 (Figures S3D and S3E; Table S4). The low detection efficacy for fusion transcripts from the scRNA-seq data might be due to the low number of reads obtained in single cells.

CTNNBIP1-CLSTN1 is highly expressed in oRGs

Of the three in-frame fusion transcripts enriched in oRGs, we focused on *CTCL*, which was expressed in multiple human tissues and cells (Babiceanu et al., 2016), including developing human cortex from early to middle gestational stages (Figure 1J). *CTCL* was identified in both poly(A)-enriched mRNAs and total RNAs from 5/8 samples (Figure 1J). In addition to the classical *CTCL*, we also found a type of protein-noncoding *CTNNBIP1-CLSTN1* fusion only in one GW23 cortical sample (Figures S3F and S3G). To further validate the presence of *CTCL* in the developing human cortex, we extracted total RNAs from a sample of GW13.3 human cortex, followed by reverse transcription and Sanger sequencing using specific primers to amplify the fragments containing fusion sites between *CTNNBIP1* and *CLSTN1* (Figures 3A and 3B). Then, we performed quantitative PCR (qPCR) to quantify the expression of *CTCL* and parental genes in sorted NPs and SATB2$^+$ neurons from samples of human cortices on GW14–GW16 (GW14.5, GW14.8, GW15.7) (Figure S1A), using *GAPDH* as an internal reference (Figure 3C). We found that *CTCL* was expressed highly in oRGs, low in
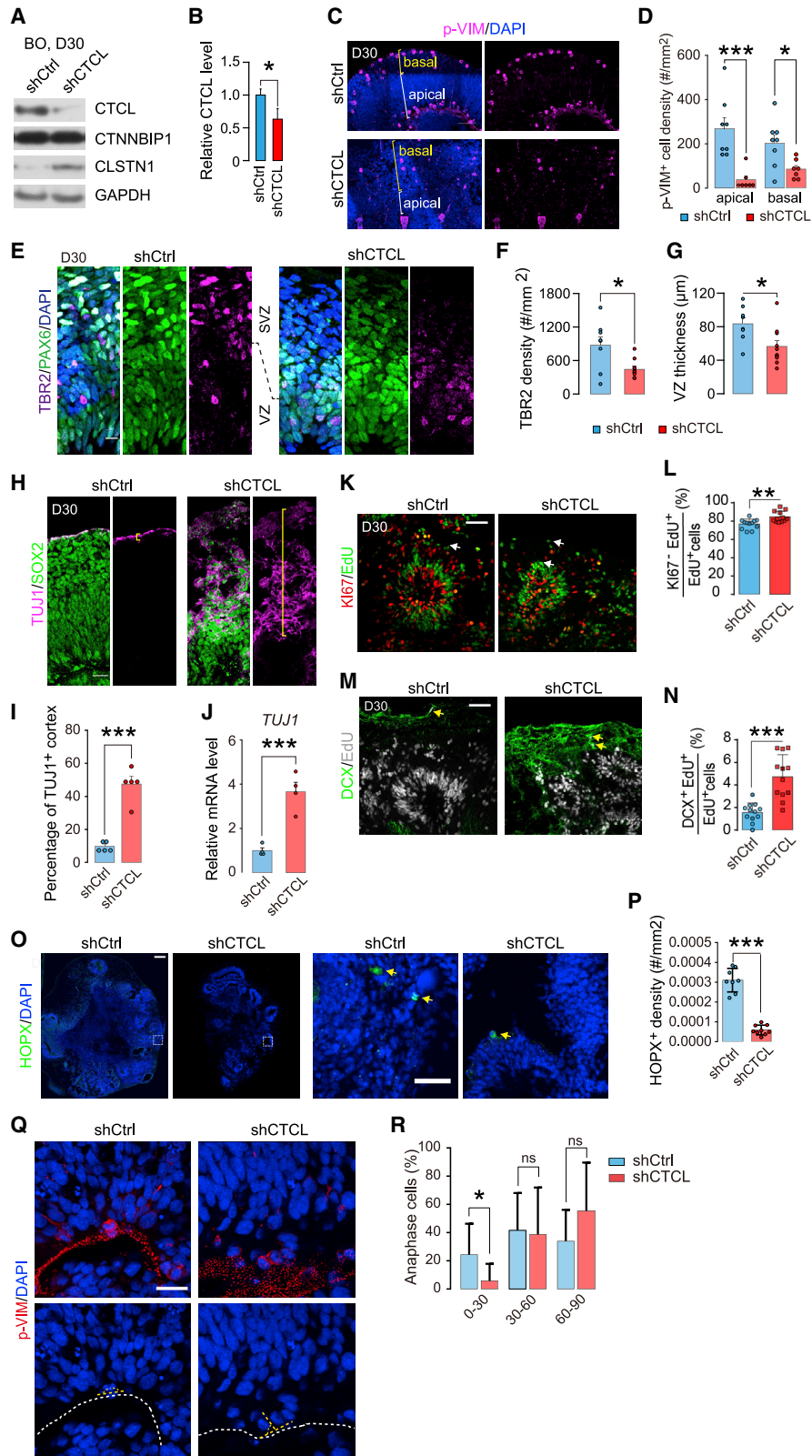
(legend on next page)

vRGs, but undetectable in IPs or neurons, and this pattern was distinct from two parental genes (Figure 3C). We also compared the expression of *CTCL* fusion mRNA in the cortices of human at GW14.5 and mice at embryonic day 14.5 (E14.5), and found that *CTCL* was undetectable in the mouse cortex (Figure 3D). This result is in line with the notion that *CTCL* was enriched in oRGs, which are abundant in primates but rare in mice.

To determine whether the *CTCL* fusion transcripts really generate in-frame fusion proteins, we performed immunoblotting (IB) with antibodies recognizing either the N terminus of CTNNBIP1 or C terminus of CLSTN1 for samples from GW14.5 human cortex (Figure 3E). Of note, both CTNNBIP1 and CLSTN1 antibodies recognized the band of predicted size (114 kDa) for the fusion protein (Figure 3E, red arrowheads). Next, we determined the presence of *CTCL* in cultured human brain organoids, which have been developed to mimic human cortex development (Lancaster and Knoblich, 2014). As shown in Figure 3F, along the course of organoid culture, the expression of *CTCL* fusion transcripts progressively increased, in particular after switch to organoid differentiation medium (Lancaster and Knoblich, 2014) at day 15. The presence and expression pattern of *CTCL* suggest its role in human cortex development.

Downregulation of *CTCL* affects neurogenesis in human brain organoids

We therefore investigated roles of *CTCL* fusion products in human cortex development by using cultured human brain organoids. First, we generated stable hESC lines expressing the short hairpin RNA specifically against *CTCL* (shCTCL) or control scrambled sequence, and examined the knockdown effects in induced brain organoids (BOs) at day 12 (Figures S4A and S4B). Compared to the control group, the shCTCL organoids exhibited marked reduction in the expression of *CTCL*, but not parental genes (Figures S4A and S4B). The knockdown effect was also validated in IB experiment for BOs at day 30 (Figures 4A and 4B).

Next, we determined the effects of *CTCL* knockdown on NP proliferation and differentiation in BOs at day 30. We first labeled dividing NPs with phosphorylated Vimentin (p-VIM). In contrast to the vRGs dividing at the apical VZ surface, oRGs and basal IPs divided in basal region of cortices (Hansen et al., 2010). We found that shCTCL organoids exhibited marked reduction in the density of p-VIM[+] progenitors, which were localized at either apical or basal regions (Figures 4C and 4D). Furthermore, the density of TBR2^{+} basal NPs, mainly IPs, was also decreased in shCTCL organoids (Figures 4E and 4F). Given that *CTCL* was barely detected in human IPs, the reduction in IPs was most likely caused by the impairment on the pool of RGs. Cortical neurons are born via direct neurogenesis from RGs or indirectly from IPs, through either symmetric or asymmetric divisions (Miyata et al., 2004; Noctor et al., 2004). The impairment in NPs in *CTCL* knockdown organoids was also reflected by reduced thickness of VZ-like regions labeled by PAX6 and devoid of TBR2 (Figures 4E and 4G). Surprisingly, in contrast to decreased SOX2^{+} progenitor pool, the band of differentiated neurons labeled by TUJ1 (β-Tubulin III) was significantly expanded (Figures 4H and 4I) and the level of *TUJ1* mRNA was also increased (Figure 4J). These results suggest that the presence of *CTCL* may maintain RGs in proliferative state, and the downregulation of *CTCL* caused precocious neuronal differentiation with the consumption of NPs. In line with this hypothesis, the overall size of the *CTCL* knockdown organoids was smaller than controls at day 30 or 60 (Figures S4C–S4E). Notably, the *CTCL* knockdown organoids displayed neurite-like processes, which extended to the peripheral Matrigel (Figures S4C and 4D). This phenomenon is reminiscent of forward shift in neuronal morphogenesis upon early onset of differentiation. In addition to reduced expansion and precocious neuronal differentiation, the *CTCL* knockdown organoids exhibited alterations in cortical niche architecture as reflected from the disruption in apical cilium and a discontinuous VZ surface (Figures S4F and 4Q). This may explain why *CTCL* knockdown organoids also

---

Figure 4. Downregulation of *CTNNBIP1-CLSTN1* impedes the development of human brain organoids

(A and B) Immunoblotting analysis for the expression of CTCL in control or shCTCL brain organoids at D30. Data are presented as representative (A) or quantitative results (B) of 3 independent experiments. *p < 0.05 (Student's t test).

(C) Slices of D30 brain organoids were immunostained with p-VIM antibody and DAPI (cell nuclei). Images shown are representative examples. The brightness difference of DAPI signals is caused by tiled scan of the whole specimen. Scale bar, 50 μm.

(D) Quantification of p-VIM[+] progenitors in the apical or basal regions of brain organoids. Data are presented as mean ± SEM of 8 control organoids and 7 shCTCL organoids. *p < 0.05, ***p < 0.001 (ANOVA with post hoc Tukey's test).

(E) Immunostaining with antibodies against TBR2 and PAX6 in organoids at D30. Dashed line indicates the boundary of VZ (ventricular zone) and SVZ (subventricular zone) in the D30 cortex-like structures. Scale bar, 10 μm.

(F and G) Quantification of TBR2^{+} IPs density (F) and VZ thickness (G) in the brain organoids. *p < 0.05 (7 shCtrl organoids and 9 shCTCL organoids; Student's t test).

(H) Immunostaining with antibodies against SOX2 and TUJ1 in organoids at D30. Yellow lines indicate the area with TUJ1^{+} neurons. Scale bar, 20 μm.

(I) Ratio of TUJ1^{+} layer to the whole thickness of cortex-like structure. *p < 0.05 (n = 4 organoids each group; Student's t test).

(J) Expression of neuronal cell marker *TUJ1* in indicated brain organoids at D30. *p < 0.05 (n = 5 organoids each group; Student's t test).

(K) Brain organoids at D30 were pulse labeled with EdU and examined 2 days later by staining with EdU (green) and KI67 (red). Scale bar, 50 μm.

(L) Quantification for the percentage of EdU[+]KI67^{−} cells among EdU^{+} cells. **p < 0.01 (at least 10 organoids each group; Mann-Whitney test).

(M) D30 organoids were pulse labeled with EdU and examined 2 days later by staining with EdU (gray) and DCX (green). Scale bar, 50 μm.

(N) Quantification for the percentage of EdU[+]DCX^{+} cells among EdU^{+} cells. ***p < 0.0001 (at least 10 organoids each group; Mann-Whitney test).

(O) Immunostaining for oRG marker HOPX (green) in D60 organoids. Scale bars, 200 μm (left) and 50 μm (magnified).

(P) Quantification of HOPX-positive cells per mm² DAPI-positive area in D60 organoids. ***p < 0.0001 (unpaired t test with Welch's correction).

(Q) D60 organoids were stained with p-VIM antibody to reveal mitotic cells in VZ-like regions of D60 organoids. Dashed lines indicate division plane (yellow) relative to VZ-surface (white). Scale bar, 20 μm.

(R) Quantification of division angle of p-VIM-positive cells at anaphase in VZ-like regions. *p < 0.05; ns, no significant difference (13 shCtrl organoids and 15 shCTCL organoids; Mann-Whitney test).

See also Figure S4.
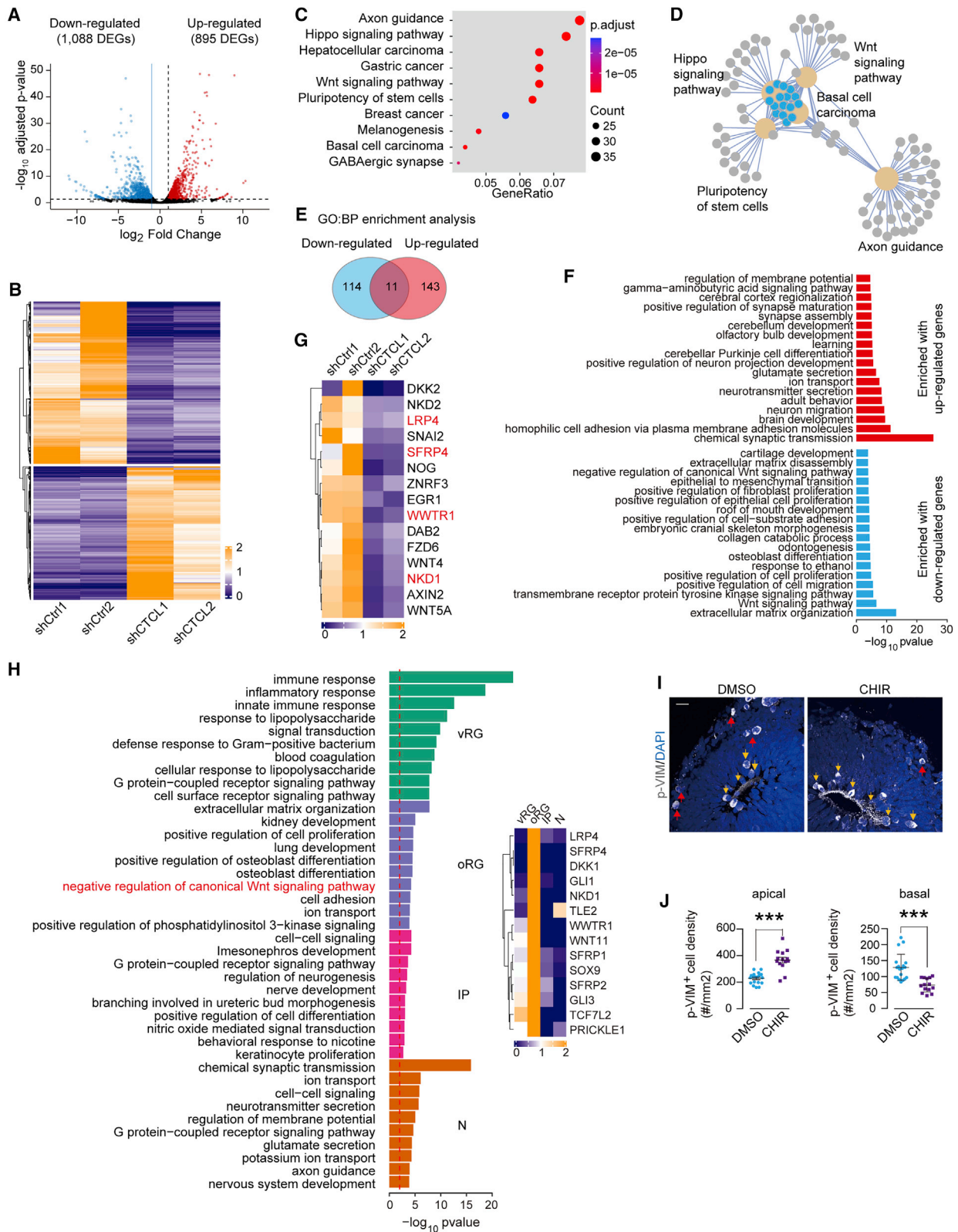
(legend on next page)

showed reduction in apical progenitors, which mainly represent vRGs (Figures 4C and 4D). Although *CTCL* was enriched in oRGs, it was still detectable in vRGs with a low level. It is possible that *CTCL* also regulates the vRG proliferation and differentiation in a cell-autonomous manner.

The extension of neurogenesis period and increased stemness of NPs are associated with human cortex expansion (Lui et al., 2011; Sun and Hevner, 2014). We determined the role of *CTCL* in cell cycle exit by pulse labeling cycling NPs with EdU, followed by staining with mitosis marker KI67 or post-mitotic neuronal marker DCX (Figures 4K and 4M). We found that the percentage of KI67⁻EdU⁺ cells among EdU⁺ cells was mildly but significantly increased in day 30 (D30) shCTCL organoids, indicating that *CTCL* knockdown had promoted cell cycle exit (Figure 4L). In line with this notion, the percentage of DCX⁺ cells among EdU⁺ cells was markedly increased (Figure 4N). We also determined the effect of *CTCL* knockdown on oRG-like cells at a later stage of organoid culture and found a reduction in HOPX-positive cells in shCTCL organoids at D60 (Figures 4O and 4P). The disruption in proliferation/differentiation balance was usually accompanied by changes in the cleavage plane orientation, as shown in cerebral organoids derived from patients/people with Miller-Dieker syndrome (MDS) (Bershteyn et al., 2017; Iefremova et al., 2017). We therefore investigated division angles of mitotic RGs labeled by p-VIM and found that vRGs at anaphase in *CTCL* knockdown organoids exhibited a significant change of the division plane, as reflected from reduced percentage of cells with horizontal division (0–30 degree) in D60 organoids and increased percentage of cells with oblique division (30–60 degree) in D30 organoids (Figures 4Q, 4R, S4G, and S4H). This tendency may not necessarily reflect switch between proliferative symmetric and neurogenic asymmetric divisions. In fact, disruption in the generation and/or proliferation of oRGs may also be reflected from the changes in the division angle. Nevertheless, these results support the conclusion that the expression of *CTCL* in human NPs is attributable to the enhanced proliferative capacity of NPs and tightly controls cell fates of daughter cells.

CTNNBIP1-CLSTN1 regulates β-catenin pathway in NPs

To understand the mechanism underlying the role of *CTCL* in regulating human cortical neurogenesis, we compared the transcriptomes of shCtrl and shCTCL organoids by analyzing the bulk RNA-seq results (Figures 5A and 5B). We found that 895 and 1,088 genes were identified upregulated and downregulated for at least 2 folds in shCTCL organoids, respectively (adjusted p value < 0.05) (Figures 5A and 5B). These differentially expressed genes (DEGs) were enriched in the categories of Hippo or Wnt signaling, pluripotency of stem cells, or axon guidance (Figures 5C and 5D), and classified into 114 biological process categories for downregulated genes only, 143 for upregulated genes only, and 11 for both (Figure 5E). Furthermore, genes promoting neuronal differentiation, maturation, and activity were upregulated in shCTCL organoids, whereas genes regulating cell proliferation were downregulated (Figure 5F). These results are in line with the finding that *CTCL* knockdown reduced NP proliferation and promoted neuronal differentiation.

The *CTCL* upstream parental gene *CTNNBIP1* encodes ICAT (inhibitor of β-catenin and T cell factor), which inhibits Wnt signaling by interfering with the interaction between β-catenin and T cell factor (TCF) (Tago et al., 2000). Interestingly, both the categories of "Wnt signaling pathway" and "negative regulation of canonical Wnt signaling pathway" were enriched in downregulated genes, but not upregulated genes, in shCTCL organoids (Figures 5F and 5G; Table S5). Several genes encoding proteins negatively regulating canonical Wnt signaling pathway, including Wnt ligands (Wnt4, Wnt5a), receptor/co-receptor (LRP4, FZD6), receptor binding proteins (DKK2, SFRP2), and signaling proteins (AXIN2), were on the list of genes downregulated in *CTCL* knockdown organoids (Figure 5G). Thus, the expression of *CTCL* fine-tunes Wnt signaling in cortical NPs. Because *CTCL* was enriched in oRGs, we wondered whether the expression patterns of Wnt signaling genes are distinct in different types of NPs as well as differentiated neurons. Notably, "negative regulation of canonical Wnt signaling pathway" was on the top GO terms enriched in oRGs, which was confirmed by different bioinformatics methodologies (Figures 5H and S5A–S5C; Table S6). Some genes highly expressed in oRGs were also observed on the panel of genes downregulated in *CTCL* knockdown organoids (Figure 5G, see genes in red). This result suggests that the presence of CTCL in oRGs fine-tunes Wnt signaling at a proper level that may be crucial for the balance of proliferation and differentiation status. In line

---

Figure 5. Impairment of Wnt signaling in CTCL knockdown brain organoids

(A) Volcano plot shows differentially expressed genes (adjusted p values < 0.05 and fold changes ≥ 2) between shCTCL and shCtrl organoids at D30.

(B) Heatmap of DEGs in shCTCL organoids compared with shCtrl organoids.

(C) The top 10 pathways enriched with differentially expressed genes.

(D) A network of enriched GO terms. Each gray dot represents single gene and blue dots represent node genes. The gene numbers of each GO term are reflected from the circle size (yellow circle).

(E) Summary for the GO biological processes (GO:BP) enriched with upregulated or downregulated genes in shCTCL organoids.

(F) Top 18 GO categories with the smallest p values.

(G) Heatmap of the 15 DEGs negatively regulating canonical Wnt signaling in shCTCL organoids. Note that some genes (red) were also highly expressed in human oRGs.

(H) The top 10 GO biological processes enriched with higher expressed genes in indicated cell populations. Red dashed line indicates the p value 0.01. The inset represents the 14 higher expressed genes negatively regulating canonical Wnt signaling pathway in oRGs.

(I) D30 cerebral organoids treated with CHIR99021 (CHIR, 3 μM) from D15 were stained with p-VIM antibody together with DAPI to mark cell distribution. Red and yellow arrows mark NPs at basal and apical regions, respectively. Scale bar, 20 μm.

(J) Quantification for the density of mitotic NPs at apical and basal regions. Data were collected from 4 independent experiments with each group having 3–5 organoids. ***p < 0.001 (unpaired t test with Welch's correction).

See also Figure S5 and Tables S5 and S6.

with this notion, the percentage of cells expressing active β-catenin was higher in vRGs compared to oRGs labeled by HOPX (Figures S5D and S5E).

To corroborate the role of Wnt/β-catenin signaling in RGs, cerebral organoids at D15 were treated for 15 days with 3 μM CHIR99021 (CHIR), which stabilizes β-catenin via inhibiting GSK3β (Naujok et al., 2014), and then analyzed at D30 for the number of mitotic NPs labeled by p-VIM (Figure 5I). Surprisingly, CHIR-treated organoids exhibited increased NPs in apical regions but decreased NPs in basal regions (Figures 5I and 5J). This result is in line with previous observation that overexpression of β-catenin in mice led to amplification of NPs at the VZ region (Chenn and Walsh, 2002), but negatively regulated basal NP populations like IPs (Mutch et al., 2010). Thus, fine-tuning of Wnt signaling is necessary for appropriate NP production, proliferation, or maintenance.

DISCUSSION

Fusion transcripts have been detected widely in normal human and mouse tissues, including the nervous system, but their physiological functions remain largely unknown, especially in the brain (Babiceanu et al., 2016; Lei et al., 2016a; Mehani et al., 2020; Singh et al., 2020; Xie et al., 2016). In this work, we identified three in-frame fusion transcripts highly expressed in oRGs, and then focused on CTCL, which was formed by fusion of mRNAs encoding N-terminal of β-Catenin binding protein ICAT and majority of Calsyntenin-1. By taking advantage of cultured human BOs, we further investigated the role of CTCL in NP proliferation and differentiation. We conclude that the presence of CTCL in NPs, in particular oRGs, is related with their enhanced self-renewal and proliferative capacity.

Unlike evolutionarily new genes, fusion transcripts that utilize existing mRNA or genes may execute a refined regulatory role in higher animals. Given that many fusions are present in distinct cell types and developmental stages, e.g., CTCL is largely enriched in oRGs, it is likely that fusion transcripts perform as temporary regulators to target pathways in a temporal and spatial manner during human neurogenesis and patterning. The mechanism of fusion transcripts generation in vivo remains largely unclear. Certain fusion transcripts are commonly formed in tumor cells as a result of chromosomal translocations (Chase et al., 2010). Recent studies have shown that fusion transcripts can also be produced by trans-splicing of intergenic/intragenic mRNAs or cis-splicing between neighboring genes (Kumar et al., 2016; Lei et al., 2016a), in normal tissues and cells in regulated manner, such as CTCL formed by cis-splicing of adjacent CTNNBIP and CLSTN1 (Babiceanu et al., 2016; Chwalenia et al., 2019). As abundant fusion transcripts are present in the developing human cortex, and many of them are in nontraditional splicing sites, it is still a challenging work to understand the role of mRNA fusions in human brain development and functions. Fusion transcripts with specific function are likely to be the product of positive selection from evolution, which extend the variety of transcriptome.

β-catenin (CTNNB1) is known to be a component in the adherens junctions that maintain tissue architecture of the neuroepithelium (Junghans et al., 2005; Machon et al., 2003) and also a

transcriptional coactivator downstream of the canonical Wnt signaling pathway (Nelson and Nusse, 2004). The role of β-catenin in regulating NP proliferation versus differentiation has been extensively studied in rodents, but the conclusions are complicated, largely owing to its multifunctional roles. For example, transgenic mice expressing a stabilized form of β-catenin in NPs lead to increased cell cycle reentry and expansion of NPs in the VZ (Chenn and Walsh, 2002) and inhibition of β-catenin-mediated transcription promotes premature exit of cell cycle, leading to precocious neuronal differentiation (Woodhead et al., 2006). In addition, Wnt/β-catenin pathway has been shown to have differential effects on distinct types of cortical NPs, enhancing vRG proliferation and IP differentiation (Munji et al., 2011). A recent study showed that deregulation and high tone of β-catenin signaling caused by deletion of adenomatous polyposis coli (APC) disrupted cortical NP proliferation and caused primary cilium defects, and surprisingly, downregulating β-catenin activity rescued the defects caused by APC deletion (Nakagawa et al., 2017). Thus, maintaining β-catenin signaling at an appropriate level might be necessary for the orderly differentiation of NPs. The role of β-catenin in human cortex development has not been fully explored. A recent study modeling MDS using patient-derived forebrain organoids indicates that disruption of the VZ niche architecture, resulting from disturbance of the N-cadherin/β-catenin, may contribute to the disease (Iefremova et al., 2017). Our results show that self-renewing oRGs that presumably lack adherens junction architecture exhibit enriched expression of genes in the category of "negative regulation of canonical Wnt signaling pathway." Interestingly, downregulating the expression of CTCL fusion transcript, which is highly expressed in oRGs, led to precocious neuronal differentiation and a concurrent reduction in proliferative NPs. The dysregulated gene expression network for Wnt signaling might have caused disordered neurogenesis patterns. Given that the parental gene product CLSTN1 regulates trafficking of a variety of molecules (Alther et al., 2016; Vogt et al., 2001), it is possible that CTCL fusion may facilitate localization of ICAT activity to subcellular domains. These possibilities await further investigation.

Accumulating lines of evidence have shown roles of human-specific genomic features in evolutionary cortex expansion. Only until recently, the repertoire of fusion transcripts in normal tissues and cells has become recognized. However, their physiological functions have not been explored, in particular for brain development. This study has explored the physiological functions of fusion transcripts in human brain development. The presence of distinct fusion transcripts in various neural cell types and different species indicates mechanisms of brain development and functioning.

STAR★METHODS

Detailed methods are provided in the online version of this paper and include the following:

- KEY RESOURCES TABLES
- RESOURCE AVAILABILITY
  - Lead contact
  - Materials availability

- ○ Data and code availability
- ● EXPERIMENTAL MODEL AND SUBJECT DETAILS
  - ○ Human fetal brain samples
  - ○ Human embryonic stem cells
- ● METHOD DETAILS
  - ○ Cell isolation from fetal prefrontal cortex
  - ○ RNA sequencing and data analysis
  - ○ CTCL knockdown in H9 cells
  - ○ Brain organoid (BO) culture and EdU labeling
  - ○ Quantitative PCR (qPCR)
  - ○ Immunoblotting
  - ○ Immunohistochemistry
- ● QUANTIFICATION AND STATISTICAL ANALYSIS

REFERENCES

Alther, T.A., Domanitskaya, E., and Stoeckli, E.T. (2016). Calsyntenin 1-mediated trafficking of axon guidance receptors regulates the switch in axonal responsiveness at a choice point. Development *143*, 994–1004.

Babiceanu, M., Qin, F., Xie, Z., Jia, Y., Lopez, K., Janus, N., Facemire, L., Kumar, S., Pang, Y., Qi, Y., et al. (2016). Recurrent chimeric fusion RNAs in non-cancer tissues and cells. Nucleic Acids Res. *44*, 2859–2872.

Bershteyn, M., Nowakowski, T.J., Pollen, A.A., Di Lullo, E., Nene, A., Wynshaw-Boris, A., and Kriegstein, A.R. (2017). Human iPSC-derived cerebral or-ganoids model cellular features of lissencephaly and reveal prolonged mitosis of outer radial glia. Cell Stem Cell *20*, 435–449.e4.

Betizeau, M., Cortay, V., Patti, D., Pfister, S., Gautier, E., Bellemin-Ménard, A., Afanassieff, M., Huissoud, C., Douglas, R.J., Kennedy, H., and Dehay, C. (2013). Precursor diversity and complexity of lineage relationships in the outer subventricular zone of the primate. Neuron *80*, 442–457.

Brooks, Y.S., Wang, G., Yang, Z., Smith, K.K., Bieberich, E., and Ko, L. (2009). Functional pre-mRNA trans-splicing of coactivator CoAA and corepressor RBM4 during stem/progenitor cell differentiation. J. Biol. Chem. *284*, 18033–18046.

Chase, A., Ernst, T., Fiebig, A., Collins, A., Grand, F., Erben, P., Reiter, A., Schreiber, S., and Cross, N.C. (2010). TFG, a target of chromosome transloca-tions in lymphoma and soft tissue tumors, fuses to GPR128 in healthy individuals. Haematologica *95*, 20–26.

Chenn, A., and Walsh, C.A. (2002). Regulation of cerebral cortical size by control of cell cycle exit in neural precursors. Science *297*, 365–369.

Chwalenia, K., Qin, F., Singh, S., and Li, H. (2019). A cell-based splicing reporter system to identify regulators of cis-splicing between adjacent genes. Nucleic Acids Res. *47*, e24.

Fietz, S.A., Kelava, I., Vogt, J., Wilsch-Bräuninger, M., Stenzel, D., Fish, J.L., Corbeil, D., Riehn, A., Distler, W., Nitsch, R., and Huttner, W.B. (2010). OSVZ progenitors of human and ferret neocortex are epithelial-like and expand by integrin signaling. Nat. Neurosci. *13*, 690–699.

Finta, C., and Zaphiropoulos, P.G. (2002). Intergenic mRNA molecules result-ing from trans-splicing. J. Biol. Chem. *277*, 5882–5890.

Florio, M., Albert, M., Taverna, E., Namba, T., Brandl, H., Lewitus, E., Haffner, C., Sykes, A., Wong, F.K., Peters, J., et al. (2015). Human-specific gene ARH-GAP11B promotes basal progenitor amplification and neocortex expansion. Science *347*, 1465–1470.

Geschwind, D.H., and Rakic, P. (2013). Cortical evolution: judge the brain by its cover. Neuron *80*, 633–647.

Gu, Z., Eils, R., and Schlesner, M. (2016). Complex heatmaps reveal patterns and correlations in multidimensional genomic data. Bioinformatics *32*, 2847–2849.

Haas, B.J., Dobin, A., Li, B., Stransky, N., Pochet, N., and Regev, A. (2019). Accuracy assessment of fusion transcript detection via read-mapping and de novo fusion transcript assembly-based methods. Genome Biol. *20*, 213.

Hansen, D.V., Lui, J.H., Parker, P.R.L., and Kriegstein, A.R. (2010). Neurogenic radial glia in the outer subventricular zone of human neocortex. Nature *464*, 554–561.

Heide, M., Haffner, C., Murayama, A., Kurotaki, Y., Shinohara, H., Okano, H., Sasaki, E., and Huttner, W.B. (2020). Human-specific *ARHGAP11B* increases size and folding of primate neocortex in the fetal marmoset. Science *369*, 546–550.

Horiuchi, T., and Aigaki, T. (2006). Alternative trans-splicing: a novel mode of pre-mRNA processing. Biol. Cell *98*, 135–140.

Huang, W., Kane, J.K., and Li, M.D. (2008). Identification and characterization of a long isoform of human IFT80, IFT80-L. Biochem. Biophys. Res. Commun. *373*, 653–658.

Iefremova, V., Manikakis, G., Krefft, O., Jabali, A., Weynans, K., Wilkens, R., Marsoner, F., Brändl, B., Müller, F.J., Koch, P., and Ladewig, J. (2017). An or-ganoid-based model of cortical development identifies non-cell-autonomous defects in Wnt signaling contributing to Miller-Dieker syndrome. Cell Rep. *19*, 50–59.

Jia, W., Qiu, K., He, M., Song, P., Zhou, Q., Zhou, F., Yu, Y., Zhu, D., Nickerson, M.L., Wan, S., et al. (2013). SOAPfuse: an algorithm for identifying fusion tran-scripts from paired-end RNA-Seq data. Genome Biol. *14*, R12.

Jia, Y., Xie, Z., and Li, H. (2016). Intergenically spliced chimeric RNAs in can-cer. Trends Cancer *2*, 475–484.

Ju, X.C., Hou, Q.Q., Sheng, A.L., Wu, K.Y., Zhou, Y., Jin, Y., Wen, T., Yang, Z., Wang, X., and Luo, Z.G. (2016). The hominoid-specific gene TBC1D3 pro-motes generation of basal neural progenitors and induces cortical folding in mice. eLife *5*, e18197.

Junghans, D., Haas, I.G., and Kemler, R. (2005). Mammalian cadherins and protocadherins: about cell death, synapses and processing. Curr. Opin. Cell Biol. 17, 446–452.

Kumar, S., Razzaq, S.K., Vo, A.D., Gautam, M., and Li, H. (2016). Identifying fusion transcripts using next generation sequencing. Wiley Interdiscip. Rev. RNA 7, 811–823.

Lancaster, M.A., and Knoblich, J.A. (2014). Generation of cerebral organoids from human pluripotent stem cells. Nat. Protoc. 9, 2329–2340.

Lancaster, M.A., Renner, M., Martin, C.A., Wenzel, D., Bicknell, L.S., Hurles, M.E., Homfray, T., Penninger, J.M., Jackson, A.P., and Knoblich, J.A. (2013). Cerebral organoids model human brain development and microcephaly. Nature 501, 373–379.

Lei, Q., Li, C., Zuo, Z., Huang, C., Cheng, H., and Zhou, R. (2016a). Evolutionary insights into RNA trans-splicing in vertebrates. Genome Biol. Evol. 8, 562–577.

Li, H., Wang, J., Mor, G., and Sklar, J. (2008). A neoplastic gene fusion mimics trans-splicing of RNAs in normal human cells. Science 321, 1357–1361.

Liu, S.J., Nowakowski, T.J., Pollen, A.A., Lui, J.H., Horlbeck, M.A., Attenello, F.J., He, D., Weissman, J.S., Kriegstein, A.R., Diaz, A.A., and Lim, D.A. (2016). Single-cell analysis of long non-coding RNAs in the developing human neocortex. Genome Biol. 17, 67.

Liu, J., Liu, W., Yang, L., Wu, Q., Zhang, H., Fang, A., Li, L., Xu, X., Sun, L., Zhang, J., et al. (2017). The primate-specific gene TMEM14B marks outer radial glia cells and promotes cortical expansion and folding. Cell Stem Cell 21, 635–649.e8.

Lui, J.H., Hansen, D.V., and Kriegstein, A.R. (2011). Development and evolution of the human neocortex. Cell 146, 18–36.

Machon, O., van den Bout, C.J., Backman, M., Kemler, R., and Krauss, S. (2003). Role of beta-catenin in the developing cortical and hippocampal neuroepithelium. Neuroscience 122, 129–143.

Malatesta, P., Hartfuss, E., and Götz, M. (2000). Isolation of radial glial cells by fluorescent-activated cell sorting reveals a neuronal lineage. Development 127, 5253–5263.

McConnell, M.J., Lindberg, M.R., Brennand, K.J., Piper, J.C., Voet, T., Cowing-Zitron, C., Shumilina, S., Lasken, R.S., Vermeesch, J.R., Hall, I.M., and Gage, F.H. (2013). Mosaic copy number variation in human neurons. Science 342, 632–637.

Mehani, B., Narta, K., Paul, D., Raj, A., Kumar, D., Sharma, A., Kaurani, L., Nayak, S., Dash, D., Suri, A., et al. (2020). Fusion transcripts in normal human cortex increase with age and show distinct genomic features for single cells and tissues. Sci. Rep. 10, 1368.

Miyata, T., Kawaguchi, A., Saito, K., Kawano, M., Muto, T., and Ogawa, M. (2004). Asymmetric production of surface-dividing and non-surface-dividing cortical progenitor cells. Development 131, 3133–3145.

Munji, R.N., Choe, Y., Li, G., Siegenthaler, J.A., and Pleasure, S.J. (2011). Wnt signaling regulates neuronal differentiation of cortical intermediate progenitors. J. Neurosci. 31, 1676–1687.

Mutch, C.A., Schulte, J.D., Olson, E., and Chenn, A. (2010). Beta-catenin signaling negatively regulates intermediate progenitor population numbers in the developing cortex. PLoS ONE 5, e12376.

Nakagawa, N., Li, J., Yabuno-Nakagawa, K., Eom, T.Y., Cowles, M., Mapp, T., Taylor, R., and Anton, E.S. (2017). APC sets the Wnt tone necessary for cerebral cortical progenitor development. Genes Dev. 31, 1679–1692.

Naujok, O., Lentes, J., Diekmann, U., Davenport, C., and Lenzen, S. (2014). Cytotoxicity and activation of the Wnt/beta-catenin pathway in mouse embryonic stem cells treated with four GSK3 inhibitors. BMC Res. Notes 7, 273.

Nelson, W.J., and Nusse, R. (2004). Convergence of Wnt, beta-catenin, and cadherin pathways. Science 303, 1483–1487.

Noctor, S.C., Flint, A.C., Weissman, T.A., Dammerman, R.S., and Kriegstein, A.R. (2001). Neurons derived from radial glial cells establish radial units in neocortex. Nature 409, 714–720.

Noctor, S.C., Martínez-Cerdeño, V., Ivic, L., and Kriegstein, A.R. (2004). Cortical neurons arise in symmetric and asymmetric division zones and migrate through specific phases. Nat. Neurosci. 7, 136–144.

Nonaka-Kinoshita, M., Reillo, I., Artegiani, B., Martínez-Martínez, M.A., Nelson, M., Borrell, V., and Calegari, F. (2013). Regulation of cerebral cortex size and folding by expansion of basal progenitors. EMBO J. 32, 1817–1828.

Pertea, M., Kim, D., Pertea, G.M., Leek, J.T., and Salzberg, S.L. (2016). Transcript-level expression analysis of RNA-seq experiments with HISAT, StringTie and Ballgown. Nat. Protoc. 11, 1650–1667.

Pollen, A.A., Nowakowski, T.J., Chen, J., Retallack, H., Sandoval-Espinosa, C., Nicholas, C.R., Shuga, J., Liu, S.J., Oldham, M.C., Diaz, A., et al. (2015). Molecular identity of human outer radial glia during cortical development. Cell 163, 55–67.

Rabbitts, T.H. (1994). Chromosomal translocations in human cancer. Nature 372, 143–149.

Ren, G., Zhang, Y., Mao, X., Liu, X., Mercer, E., Marzec, J., Ding, D., Jiao, Y., Qiu, Q., Sun, Y., et al. (2014). Transcription-mediated chimeric RNAs in prostate cancer: time to revisit old hypothesis? OMICS 18, 615–624.

Serin Harmanci, A., Harmanci, A.O., and Zhou, X. (2020). CaSpER identifies and visualizes CNV events by integrative analysis of single-cell or bulk RNA-sequencing data. Nat. Commun. 11, 89.

Singh, S., Qin, F., Kumar, S., Elfman, J., Lin, E., Pham, L.P., Yang, A., and Li, H. (2020). The landscape of chimeric RNAs in non-diseased tissues and cells. Nucleic Acids Res. 48, 1764–1778.

Stahl, R., Walcher, T., De Juan Romero, C., Pilz, G.A., Cappello, S., Irmler, M., Sanz-Aquela, J.M., Beckers, J., Blum, R., Borrell, V., and Götz, M. (2013). Trnp1 regulates expansion and folding of the mammalian cerebral cortex by control of radial glial fate. Cell 153, 535–549.

Stransky, N., Cerami, E., Schalm, S., Kim, J.L., and Lengauer, C. (2014). The landscape of kinase fusions in cancer. Nat. Commun. 5, 4846.

Sun, T., and Hevner, R.F. (2014). Growth and folding of the mammalian cerebral cortex: from molecules to malformations. Nat. Rev. Neurosci. 15, 217–232.

Tago, K., Nakamura, T., Nishita, M., Hyodo, J., Nagai, S., Murata, Y., Adachi, S., Ohwada, S., Morishita, Y., Shibuya, H., and Akiyama, T. (2000). Inhibition of Wnt signaling by ICAT, a novel beta-catenin-interacting protein. Genes Dev. 14, 1741–1749.

Tang, Y., Qin, F., Liu, A., and Li, H. (2017). Recurrent fusion RNA DUS4L-BCAP29 in non-cancer human tissues and cells. Oncotarget 8, 31415–31423.

Thomsen, E.R., Mich, J.K., Yao, Z., Hodge, R.D., Doyle, A.M., Jang, S., Shehata, S.I., Nelson, A.M., Shapovalova, N.V., Levi, B.P., and Ramanathan, S. (2016). Fixed single-cell transcriptomic characterization of human radial glial diversity. Nat. Methods 13, 87–93.

Vogt, L., Schrimpf, S.P., Meskenaite, V., Frischknecht, R., Kinter, J., Leone, D.P., Ziegler, U., and Sonderegger, P. (2001). Calsyntenin-1, a proteolytically processed postsynaptic membrane protein with a cytoplasmic calcium-binding domain. Mol. Cell. Neurosci. 17, 151–166.

Woodhead, G.J., Mutch, C.A., Olson, E.C., and Chenn, A. (2006). Cell-autonomous beta-catenin signaling regulates cortical precursor proliferation. J. Neurosci. 26, 12620–12630.

Wu, C.S., Yu, C.Y., Chuang, C.Y., Hsiao, M., Kao, C.F., Kuo, H.C., and Chuang, T.J. (2014). Integrative transcriptome sequencing identifies trans-splicing events with important roles in human embryonic stem cell pluripotency. Genome Res. 24, 25–36.

Xie, Z., Babiceanu, M., Kumar, S., Jia, Y., Qin, F., Barr, F.G., and Li, H. (2016). Fusion transcriptome profiling provides insights into alveolar rhabdomyosarcoma. Proc. Natl. Acad. Sci. USA 113, 13126–13131.

Yoshihara, K., Wang, Q., Torres-Garcia, W., Zheng, S., Vegesna, R., Kim, H., and Verhaak, R.G. (2015). The landscape and therapeutic relevance of cancer-associated transcript fusions. Oncogene 34, 4845–4854.

Zhong, S., Zhang, S., Fan, X., Wu, Q., Yan, L., Dong, J., Zhang, H., Li, L., Sun, L., Pan, N., et al. (2018). A single-cell RNA-seq survey of the developmental landscape of the human prefrontal cortex. Nature 555, 524–528.

STAR★METHODS

KEY RESOURCES TABLES

REAGENT or RESOURCE	SOURCE	IDENTIFIER
Antibodies		
Mouse anti-CRYAB	Abcam	Cat.# ab13496; RRID: AB_300400
Sheep anti-TBR2	R&D Systems	Cat.# AF6166; RRID: AB_10569705
Rabbit anti-HOPX	Sigma-Aldrich	Cat.# HPA030180; RRID: AB_10603770
Rabbit anti-SATB2	Abcam	Cat.# ab69995; RRID: AB_2285610
HRP-conjugated secondary antibodies	Millipore	Cat.# AP124P; RRID: AB_90456 Cat.# AP132P; RRID: AB_90264
Mouse anti-GAPDH	Proteintech	Cat.# 60004-1-Ig; RRID: AB_2107436
Rabbit anti-CLSTN1	Abcam	Cat.# ab134130
Rabbit anti-TUJ1	Biolegend	Cat.# 802001; RRID: AB_2564645
Mouse anti-p-VIM	MBL	Cat.# D076-3; RRID: AB_592963
Goat anti-SOX2	Santa Cruz	Cat.# sc-17319; RRID: AB_661259
Rabbit anti-PAX6	Anaspec	Cat.# PRB-278P; RRID: AB_291612
Mouse anti-KI67	BD Biosciences	Cat.# 550609; RRID: AB_393778
Goat anti-DCX	Santa Cruz	Cat.# sc-8066; RRID: AB_2088494
Rabbit anti-CTNNBIP1	Abcam	Cat.# ab129011; RRID: AB_11140197
Bacterial and virus strains		
pLenti-U6-shRNA-EF1a-EGFP-3FL AG-PGK-Puro	OOBIO	https://www.obiosh.com/
pLenti-U6-shCTCL-EF1a-EGFP-3FL AG-PGK-Puro	This manuscript	N/A
pLenti-U6-shCtrl-EF1a-EGFP-3FL AG-PGK-Puro	This manuscript	N/A
Biological samples		
GW14.5 human fetal brain	This manuscript	N/A
GW14.8 human fetal brain	This manuscript	N/A
GW15.7 human fetal brain	This manuscript	N/A
Gw13.3 human fetal brain	This manuscript	N/A
GW17 human fetal brain	This manuscript	N/A
Chemicals, peptides, and recombinant proteins		
Leibovitz L-15 medium	GIBCO	Cat.# 21083027
HEPES	Sigma-Aldrich	Cat.# H4034-100G
Bovine Serum Albumin	Sigma Aldrich	Cat.# A9418
TTX	Alomone Labs	Cat.# T-550
DNQX	Tocris	Cat.# 0189/10
DNase I	Roche	Cat.# 10104159001
DL-AP5	Tocris	Cat.# 3693/10
Antibiotic-Antimycotic	Invitrogen	Cat.# 15240096
trypsin inhibitor	Sigma-Aldrich	Cat.# T6414-100ML
RNaseOUT	Life Technologies	Cat.# 10777019
Paraformaldehyde	Sigma-Aldrich	Cat.# 158127-500G
PKD solution	QIAGEN	Cat.# 1034963
hESC-qualified Matrigel	BioCoat	Cat.# 354277
Growth factor reduced (GFR) basement membrane matrigel	BioCoat	Cat.# 354230
mTeSR1 medium	STEMCELL	Cat.# 85875

(Continued on next page)

Continued

REAGENT or RESOURCE	SOURCE	IDENTIFIER
ReLeSR	STEMCELL	Cat.# 05872
Puromycin	Sigma-Aldrich	Cat.# P8833-10MG
Y27632	Tocris	Cat.# 1254/10
Lipiture	NOF CORPORATTON	Cat.# lipiture-CM5206
Knockout Serum Replacer	Invitrogen	Cat.# 10828028
MEM-NEAA	Invitrogen	Cat.# 11140050
Dorsomorphine	Tocris	Cat.# 0102/10
A83-01	Tocris	Cat.# 2939/10
N2 Supplement	Invitrogen	Cat.# 17502048
Heparin	Sigma-Aldrich	Cat.# H3149-100KU
SB431542	Selleck	Cat.# S1067
LDN193189	Selleck	Cat.# S2618
Neurobasal	GIBCO	Cat.# 21103-049
B27 supplement	Invitrogen	Cat.# 17504044
B27 supplement without vitamin A	Invitrogen	Cat.# 12587010
Insulin	Sigma-Aldrich	Cat.# I9278
EdU	Invitrogen	Cat.# C10640
Protease inhibitor cocktail	Millipore	Cat.# 539134-1SETCN
Glutamax	GIBCO	Cat.# 35050061
DMEM:F12	GIBCO	Cat.# 11330-032
Critical commercial assays		
HiPure Total RNA Micro/Mini Kit	Magen	Cat.# R4111-02
GoScript Reverse Transcription Kit	Promega	Cat.# A5001
miRNeasy FFPE Kit	QIAGEN	Cat.# 217504
SMRTbell Express Template Prep Kit 2.0	Pacific Biosciences	Kit Insert PN: 101-685-400
Small RNA Library Prep Set for Illumina	New England Biolabs	Cat.# E7300
Deposited data		
RNA-seq (shCTCL versus shCtrl)	This manuscript	GEO: GSE155130
RNA-seq (sorted cells)	This manuscript	GEO: GSE156851
Experimental models: Cell lines		
Human ES line H9	iMedCell	http://www.cell-nest.com/page1?_l=en
Oligonucleotides		
CTNNBIP1-forward: GGAAGAGTCCGGAGGAGATGTACATTC	Invitrogen	N/A
CTNNBIP1-reverse: CTACTGCCTCCGGTCTTCCGTCT	Invitrogen	N/A
CLSTN1-forward: TCCTCCTTGGACCCCCGGAG	Invitrogen	N/A
CLSTN1-reverse: CCACAAATCTCACCTTCTTTGGTGAC	Invitrogen	N/A
CTCL-forward: GGAAGAGTCCGGAGGAGATGTACATTC	Invitrogen	N/A
CTCL-reverse:CCACAAATCTCACCTTCTTTGGTGAC	Invitrogen	N/A
Software and algorithms		
ComplexHeatmap	GitHub	https://github.com/jokergoo/ComplexHeatmap; RRID: SCR_017270
ggplot2	CRAN	https://github.com/tidyverse/ggplot2; RRID: SCR_014601

(*Continued on next page*)

Continued

REAGENT or RESOURCE	SOURCE	IDENTIFIER
SOAPfuse	SourceForge	https://sourceforge.net/p/summary/; RRID: SCR_000078
Hisat2	GitHub	https://github.com/DaehwanKimLab/hisat2; RRID: SCR_015530
StringTie	The Center for Computational Biology at Johns Hopkins University	https://ccb.jhu.edu/software/stringtie/; RRID: SCR_016323
Ballgown	Bioconductor	http://bioconductor.org/packages/release/bioc/html/ballgown.html
DESeq2	Bioconductor	http://bioconductor.org/packages/devel/bioc/html/DESeq2.html; RRID: SCR_015687
goSTAG	Bioconductor	https://www.bioconductor.org/packages/devel/bioc/html/goSTAG.html
seqLogo	Bioconductor	https://www.bioconductor.org/packages/devel/bioc/html/seqLogo.html
STAR-Fusion	GitHub	https://github.com/STAR-Fusion/STAR-Fusion/wiki#RunnningStarF
CaSpER	Bioconductor	https://www.bioconductor.org/packages/devel/bioc/html/casper.html
STAR	GitHub	https://github.com/alexdobin/STAR
Samtools	MIT	https://github.com/samtools/samtools
snpEff	GitHub	https://github.com/pcingola/SnpEff; RRID: SCR_005191
snpSift	GitHub	https://github.com/pcingola/SnpSift; RRID: SCR_015624
ImageJ (Fiji)	NIH	https://imagej.nih.gov/ij/docs/guide/146-2.html; RRID: SCR_003070
R (v3.6.0)	The R Foundation	https://www.r-project.org

RESOURCE AVAILABILITY

Lead contact
Further information and requests for resources and reagents should be directed to and will be fulfilled by the lead contact, Professor Zhen-Ge Luo (luozhg@shanghaitech.edu.cn).

Materials availability
All unique/stable reagents generated in this study are available from the lead contact with a completed materials transfer agreement.

Data and code availability
The Gene Expression Omnibus (GEO) numbers for the bulk RNA-seq of sorted neural cells and organoids in this paper are GEO: GSE156851 and GSE155130. All software used is open and freely available. The published article includes main datasets generated during this study. The remaining unpublished data and code are available from authors upon reasonable request.

EXPERIMENTAL MODEL AND SUBJECT DETAILS

Human fetal brain samples
The five human fetal brain tissue samples (see Figure S1A), including four males at GW13.3, GW14.5, GW14.8 and GW17.0 as well as one at GW15.7 with unknown sex, were collected within 3 hr of spontaneous abortion with the informed consent of the patients following protocols and institutional ethic guidelines approved by ethics committee of Shanghai Institutes for Biological Sciences, Chinese Academy of Sciences (Approval identifier number: ER-SIBS-221506). Brain tissues were stored in ice-cold Leibowitz-15 medium and transported to the laboratory for further examination and processing.

Human embryonic stem cells
Human ES line H9 (iMedCell) was cultured at 37°C with 5% CO_2 on hESC-qualified Matrigel in mTeSR1 medium (STEMCELL), checked daily for differentiation and passaged every 3-4 days with enzyme-free passaging reagent ReLeSR (STEMCELL), following the manufacture's procedure. The cells between passages 6 and 18 after purchasing from iMedCell were used in this study.

METHOD DETAILS

Cell isolation from fetal prefrontal cortex

Isolation of neural cell populations were mainly conducted as described previously (Thomsen et al., 2016). Prefrontal cortex tissue was moved into ice-cold ACSF containing 125 mM NaCl, 5 mM KCl, 1.25 mM NaH$_2$PO$_4$, 1 mM MgSO$_4$, 2 mM CaCl$_2$, 25 mM NaHCO$_3$ and 20 mM D-(+)-glucose (pH 7.4, 310 mOsm1^{-1}), bubbled with 95% O2 and 5% CO2. For cell dissociation, tissues were minced into small pieces with a razor blade in ice-cold ACSF, then digested in 2 mL trypsin solution (Ca^{2+}/Mg^{2+}-free HBSS, 10 mM HEPES, 2 mM MgCl2, 0.25 mg/ml bovine pancreatic trypsin, 10 g/ml DNase I, 100 nM TTX, 20 μM DNQX and 50 μM DL-AP5) for 20 min at 37°C. Digestion was stopped with 6 mL of ice-cold quenching buffer [88% Leibovitz L-15 medium, 50 mL sterilized double-distilled H$_2$O, 5 mL 1 M HEPES (pH 7.4), 5 mL 100x Antibiotic-Antimycotic, 2 mg/ml bovine serum albumin, 100 μg/ml trypsin inhibitor, 10 μg/ml DNase I, 100 nM TTX, 20 μM DNQX, and 50 μM DL-AP5]. Digested tissues were pelleted by centrifuge (220 g, 4 min, 4°C), suspended with 2 mL of quenching buffer and pipetted (∼25 cycles) with a 1 mL tip into single cells on ice. Cell suspension was diluted with 10 mL staining medium [88% Leibovitz L-15 medium, 50 mL sterilized double-distilled H$_2$O, 5 mL 1 M HEPES (pH 7.4), 5 mL 100x Antibiotic-Antimycotic, 20 mL 77.7 mM EDTA pH 8.0, 1 g BSA, 100 nM TTX, 20 μM DNQX, and 50 μM DL-AP5], filtered through a 70 μm cell strainer, pelleted (220 g, 10 min, 4°C), re-suspended in 5 mL ice-cold staining medium. After washes, cells were re-suspended in RNase-free staining buffer [1 × PBS, 1% RNase-free BSA (Gemini Bioproducts), 0.0025% RNaseOUT (Life Technologies), pH = 7.4]. Finally, single-cell suspension were fixed with 4% PFA (Sigma-Aldrich) in 1 × PBS on ice for 15 min, pelleted by centrifugation (335 g, 3 min, 4°C), followed by washes with 1 mL SB again and resuspension in SB at ∼10^7 cells/ml. Fixed cell aliquots were stored at −80°C.

For cell isolation, fixed cells (∼10^7) were thawed on ice and permeated with 0.1% Triton X-100 in SB, then incubated with primary antibodies diluted in SB overnight at 4°C. Antibodies used were: anti-CRYAB (Abcam, ab13496) and anti-TBR2 (R&D Systems, AF6166) for vRGs, anti-HOPX (Sigma-Aldrich, HPA030180) and anti-CRYAB for oRGs, anti-TBR2 for IPs, anti-SATB2 (Abcam, ab69995) and anti-TBR2 for neurons. Cells were washed with SB and then incubated with secondary antibodies conjugated with Alexa 488 or Alexa-555 (Life technologies) for 1 hr at 4°C, washed with SB and re-suspended in SB before sorting.

Cell sorting was carried out using the MoFlo XDP Sorter (Beckman Coulter): CRYAB$^+$/TBR2$^-$ cells as vRGs; HOPX$^+$CRYAB$^-$ cells as oRGs; TBR2$^+$ cells as IPs; SATB2$^+$/TBR2$^-$ cells as neurons. Cells were sorted into the SB solution, pelleted and re-suspended with 100 μL of PKD solution (QIAGEN). Total RNA was purified using the miRNeasy FFPE Kit (QIAGEN) according to the manufacture's protocol. 200 ng RNA of each cell population was used to analyze RNA-seq using HiSeq 4000.

RNA sequencing and data analysis

We used *SOAPfuse* software to identify fusion transcripts in human RNAs from sorted cell populations and single oRG cells (Jia et al., 2013; Liu et al., 2017; Zhong et al., 2018). Positive fusion transcripts identified using *SOAPfuse* were selected with alignment of both Junc_reads and Span_reads. The expression level of fusion transcripts was reflected from SPMR value (splicing events per million mapped reads). To analyze the differentially expressed genes in human samples, raw reads were first mapped to the hg19 human genome reference sequence by *Hisat2* software, then transcripts were assembled with *StringTie* and differentially expressed genes were identified using the *R* package *Ballgown* as described previously (Pertea et al., 2016). Alternatively, *StringTie/prepDE.py* was also used to count genes in human cell populations and DESeq2 R package was then used to normalize the gene count across populations (Figure S5A). Hisat2/*StringTie/prepDE.py* pipeline was used to count genes in sequenced organoid RNAs and then *DESeq2 R* package was used to identify differentially expressed genes. For GO enrichment analysis without statement of R packages, human GO database on biological process was obtained with the *loadGOTerm* function in the *goSTAG* R package including 18,446 genes in 3,599 GO categories of biological processes. Binomial test was used to examine whether differentially expressed genes are enriched in each GO category. The position weight matrix of the 20 bp DNA sequence motif around the fusion site was calculated by the *seqLogo* R package.

The long reads sequencing was approached by Pacific Biosciences (PacBio) platform. Briefly, full length cDNA of GW17 cortex tissue was generated by SMARTer PCR cDNA Synthesis Kit (Clontech), and processed to generate library via SMRTbell Template Prep Kit. SMRTBell libraries were sequenced on a PacBio RS II with Sequel Sequencing Kit 2.0. Ribosome-protected mRNA fragments were generated from total RNA of GW17 cortex tissue after RNase digestion and ribosome removal, and processed to construct library with Multiplex Small RNA Library Prep Set (New England Biolabs). Ribosome profiling sequencing (Ribo-seq) was performed on Illumina platform in 150 bp, paired-end mode. Fusion transcripts from long reads and Ribo-seq were then identified by the *STAR-Fusion* software from the Trinity Cancer Transcriptome Analysis Toolkit (Haas et al., 2019). Positive fusions with both Junc_reads and Span_reads or with at least three Junc_reads from Ribo-seq were considered as positive.

To check the genomic abnormality of the human specimen used for sorting cortical cell populations, we identified possible large-scale chromosomal copy number variations (CNVs) and single nucleotide polymorphism (SNPs) from RNA-seq reads. The CNV content was searched from RNA-seq data using the *CaSpER* R package (Serin Harmanci et al., 2020) through integrating the multiscale smoothing of expression signal and allelic shift signals in comparison to the average of reference genomes (GSE156988) for CNV calling. To identify the SNPs, raw reads of cell populations were first mapped to the human GRCh38 reference genome using the 2-pass mapping (STAR) and then 1,824,585 raw variants (SNPs and indels) were identified in the four cell populations using the *Samtools*. 417,122 clean variants were filtered according to the following criteria: happened in > 75% genotyped individuals, 30

for minimum quality score, 3 for minor allele count, 3 for minimum mean depth. Clean variants were annotated using snpEff and snpSift softwares and 3,039 missense/stop-gained variations were identified. Among them, 2,350 variations were found in all four cell populations and all of them are heterozygous. 18 heterozygous variations causing stop-gain mutation were identified from the GW14.5 specimen (Figure S3C), but none of them regulates the alternative splicing.

CTCL knockdown in H9 cells
RNA interference oligo against CTCL (5′-TGCTTGTTAACCTGGTCGA-3′) was cloned into lentivirus vector (pLenti-U6-shRNA-EF1a-EGFP-3FLAG-PGK-Puro). H9 cells were infected with 10^5 lentiviruses for 24 hr, followed by washes with fresh mTeSR1 medium, and treatment with 1 μg/ml Puromycin (Sigma-Aldrich) for 3 days to select virus-infected cell clones. H9 clones were digested with Accutase into single-cell suspension, then seeded and cultured in Matrigel-coated 10-cm dish (Corning) in mTeSR1 containing 10 μM Y27632 to induce clone formation. ES clones were digested with 1 mg/ml collagenase IV, moved into plates coated with Matrigel. Expressions of *CTCL*, *CTNNBIP1* and *CLSTN1* in ES clones and corresponding brain organoids were analyzed by quantitative PCR.

Brain organoid (BO) culture and EdU labeling
hES colonies were dissociated into single-cell suspension with Accutase, and then 5,000 cells were plated into each well of the lipidure-coated V-bottom 96-well plate in 150 μL mTeSR1 medium supplemented with 10 μM ROCK inhibitor Y27632 for embryoid body (EB) formation. At day 2, EBs were transferred into the stem cell medium containing 20% Knockout Serum Replacer (GIBCO), 1 × MEM-NEAA (GIBCO), 3.5 μl/L β-mercaptoenthanol (Sigma-Aldrich), 1xGlutamax (GIBCO), 2.5 μM Dorsomorphine (Tocris), 2 μM A83-01 (Tocris), in DMEM/F12 and fed every other day. At day 6, the culture medium was replaced with the neural induction medium containing 1 × N2 Supplement (GIBCO), 1 × Glutamax (GIBCO), 1xMEM-NEAA (GIBCO) and 1 μg/ml heparin (Sigma-Aldrich) in DMEM/F12 (Lancaster et al., 2013), containing 10 μM SB431542, 200 nM LDN193189 (Selleck), to induce the formation of brain organoids. At day 12, organoids were embedded in growth factor-reduced Matrigel and cultured in the neural differentiation medium (1:1 mixture of DMEM/F12: Neurobasal containing 0.5 × N2 supplement, 0.5 × B27 supplement, 3.5 μl/L β-mercaptoenthanol, 250 μl/L Insulin (Sigma-Aldrich, I9278), 1 × Glutamax and 0.5 × MEM-NEAA, 1 × Anti-Anti), according to the method reported previously (Lancaster et al., 2013). B27 supplement without vitamin A (Invitrogen, 12587010) were used in the differentiation medium for 4 days to promote the cortical expansion and then transferred into flasks containing B27 (Invitrogen, 17504044), which were then cultured on a shaker for following days with medium renewed every 2-4 days. To label proliferative progenitors, organoids were treated with 10 μM EdU (Sigma-Aldrich) for 2 hr, followed by extended culture in neural differentiation medium for 2 days. Immunofluorescence of EdU was determined following manufacturer's protocol (Abcam).

Quantitative PCR (qPCR)
Total RNA was purified from 2-4 organoids using the HiPure Total RNA Micro/Mini Kit and stored at −80°C in RNase-free H_2O containing RNase inhibitor (1 U/ml), followed by reverse transcription to form cDNA with GoScript Reverse Transcription Kit. Relative mRNA expression was determined by quantitative PCR using the Agilent Mx3000P qPCR system with primers for individual transcripts: *CTCL* (forward, 5′-GGAAGAGTCCGGAGGAGATGTACATTC-3′; reverse, 5′-CCACAAATCTCACCTTCTTTGGTGAC-3′), *CTNNBIP1* (forward, 5′- GGAAGAGTCCGGAGGAGATGTACATTC −3′; reverse, 5′- CTACTGCCTCCGGTCTTCCGTCT-3′), *CLSTN1* (forward, 5′-TCCTCCTTGGACCCCCGGAG-3′; reverse, 5′-CCACAAATCTCACCTTCTTTGGTGAC-3′). Data is presented as mean ± SEM from at least 3 biological replicates for each group, using *GAPDH* as internal control.

Immunoblotting
The homogenates of tissues or cells containing Protease Inhibitor Cocktail (Millipore, 539134-1SETCN) were denatured in 5x SDS sample buffer for 10 min at 95°C, and proteins were separated by SDS-PAGE and then transferred onto 0.45 μm PVDF membranes. After blocking in 5% milk, the membranes were incubated with primary antibodies at 4°C overnight, and then HRP-conjugated secondary antibodies (Millipore, AP124P, AP132P) for 1-2 hr at room temperature. All antibodies were diluted in 3% BSA/TBST. The primary antibodies were mouse anti-GAPDH (Proteintech, 60004-1-Ig), rabbit anti-CLSTN1 (Abcam, ab134130), and rabbit anti-CTNNBIP1 (Abcam, ab129011).

Immunohistochemistry
Human brain organoids were fixed in 4% PFA in cold PBS for at least 20 min, dehydrated by 20%–30% sucrose in PBS overnight at 4°C, imbedded in O.C.T. compound and sectioned into 30 μm slices. To achieve high quality staining, sections were subjected to heat-induced antigen retrieval using 10 mM sodium citrate (pH = 6.0) for 10 min, and permeated in 0.5% (v/v) Triton X-100 in PBS for 30-60 min at room temperature. After blocking with 5% BSA in PBS for 1 hr, sections were incubated with primary antibodies at 4°C for 48 hr and then appropriate secondary antibodies conjugated with Alexa 488, 555, or 647 for 1-2 hr at room temperature or overnight at 4°C. Primary antibodies used were: rabbit anti-TUJ1 (Biolegend, 802001), mouse anti-p-VIM (MBL, D076-3), goat anti-SOX2 (Santa Cruz, sc-17319), rabbit anti-PAX6 (Anaspec, PRB-278P), sheep anti-TBR2 (R&D, AF6166), mouse anti-KI67 (BD, 550609), and goat anti-DCX (Santa Cruz, sc-8066). Stained sections were mounted with fluorescent mounting medium and stored at 4°C before imaging. All images were acquired by confocal imaging systems.

QUANTIFICATION AND STATISTICAL ANALYSIS

Heatmap was plotted with the R package *ComplexHeatmap* (Gu et al., 2016). All plots were drawn with R package *ggplot2*. Images were measured using Fiji. For the data passing through normality and homogeneity of variances tests, unpaired t test was used for the comparison between two groups and ANOVA Tukey test was used for multiple comparison. Otherwise, rank-sum test was used. Data were presented as mean ± SEM. $*p < 0.05$, $**p < 0.01$, $***p < 0.001$. All of the statistical details of experiments can be found in the figure legends, including the statistical tests used and exact values and representations of biological replicates.